Supporting Information

Well-Dispersed and Porous FeP@C Nanoplates with Stable and Ultrafast Lithium Storage Performance through Conversion Reaction Mechanism

Fei Han,*[,a] Chengzhi Zhang,[a] Jianxiao Yang,[a] Guozhi Ma,[a] Kejian He[b] and Xuanke Li*[,a]

[a] College of Materials Science and Engineering, Hunan University, Changsha, Hunan 410082, China

[b] Advanced Research Center, Central South University, Changsha, Hunan 410082, China

*Corresponding author, Tel: +86-88821478, e-mail: feihan@hnu.edu.cn; xuankeli@hnu.edu.cn

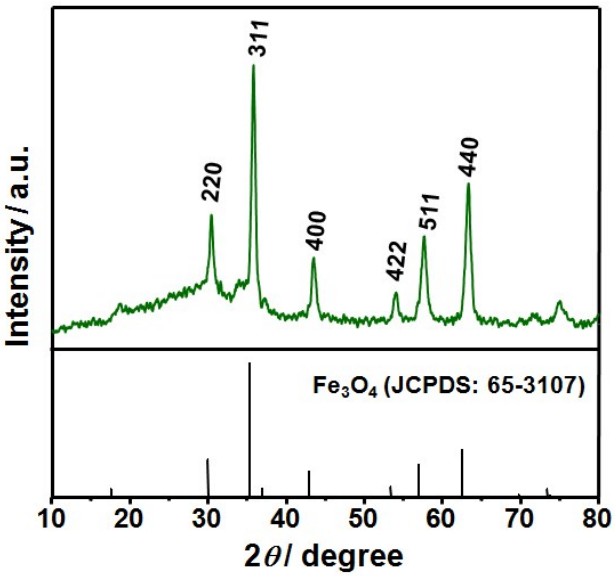

Figure S1. Wide-angle XRD patterns of Fe_3O_4@C intermediates.

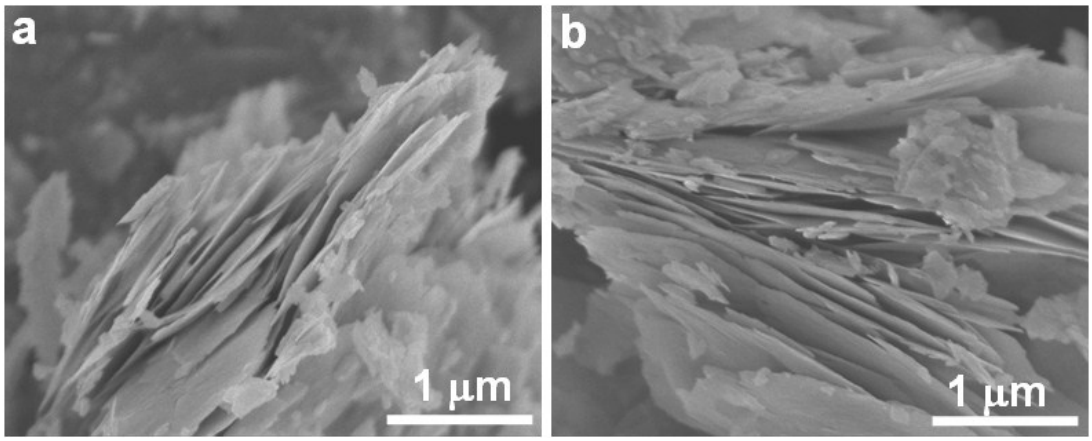

Figure S2. SEM images of Fe_2O_3 nanoplate precursors after drying, which show the severe aggregation of nanoplates.

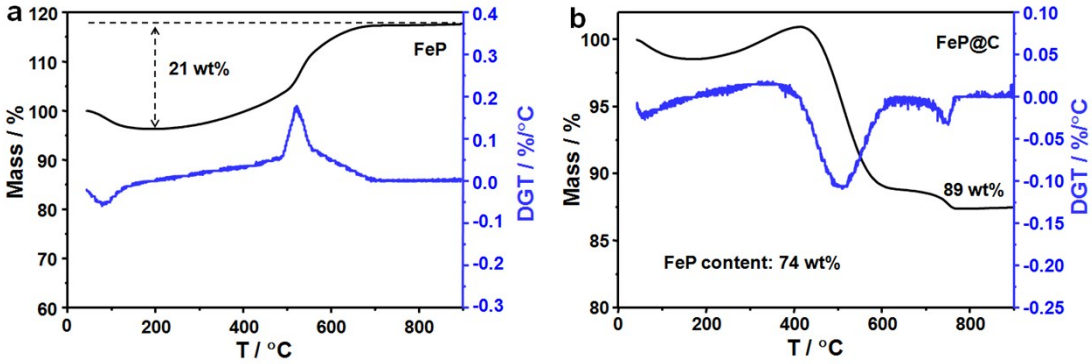

Figure S3. Thermogravimetric curves of (a) pure FeP and (b) FeP@C nanoplates thermally treated in air.

Thermogravimetric (TG) analysis was used to quantify the content of active material FeP in the FeP@C nanoplates. In both cases, the first weight loss before 200 °C corresponds to the loss of the surface adsorbed water molecules. The TG curve of pure FeP show obvious weight increase in the range of 200 to 700 °C, which is related to the gradual oxidation of FeP to Fe_2O_3 and P_2O_5. For FeP@C, the drastic weight loss from 400 to 750 °C is attributed to the burning of carbon component. Considering the oxidation of FeP and burning of carbon in the composites, the content of active material FeP in the FeP@C nanoplates is calculated to be 74 wt%.

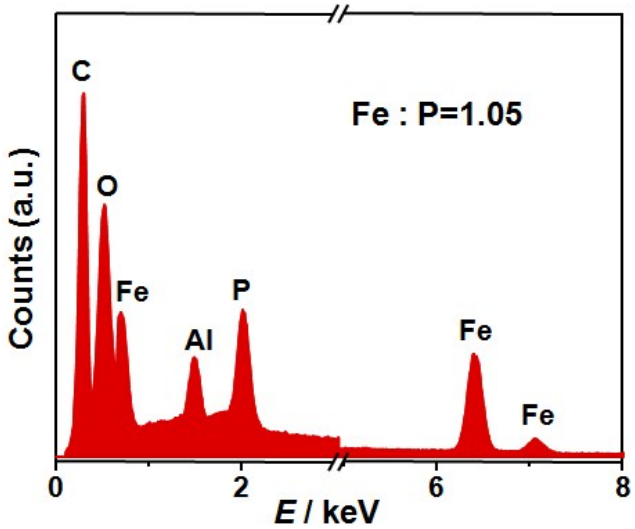

Figure S4. EDS pattern of FeP@C nanoplates with a Fe:P atomic ratio of 1.05:1.

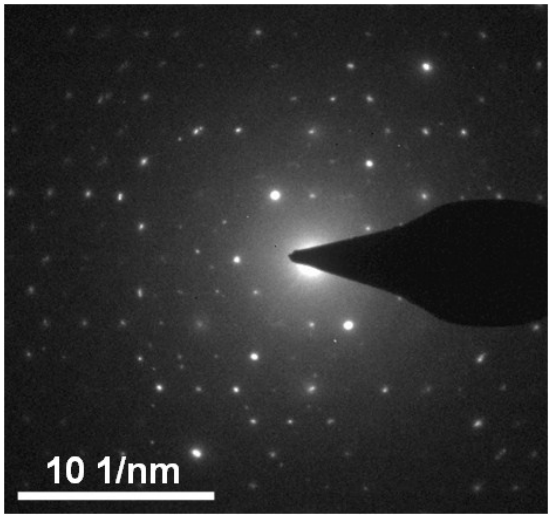

Figure S5. The SAED pattern of FeP@C nanoplates.

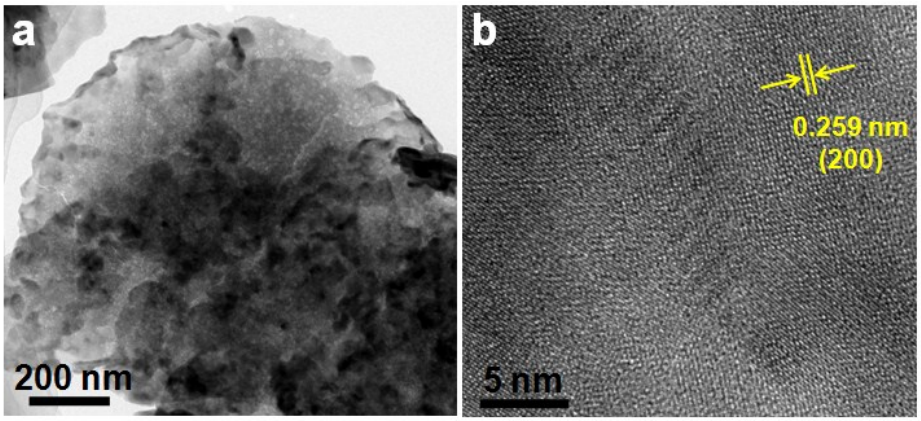

Figure S6. (a) TEM and HR-TEM images of pure FeP without carbon coating.

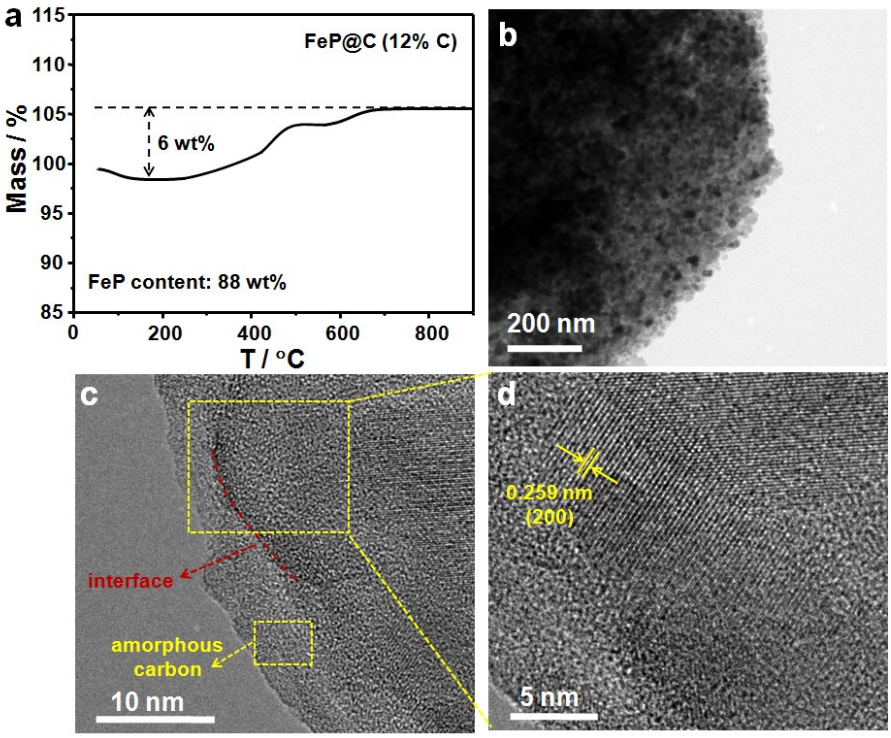

Figure S7. (a) TG curve, (b) TEM and (c,d) HR-TEM images of FeP@C with 12 wt% carbon content.

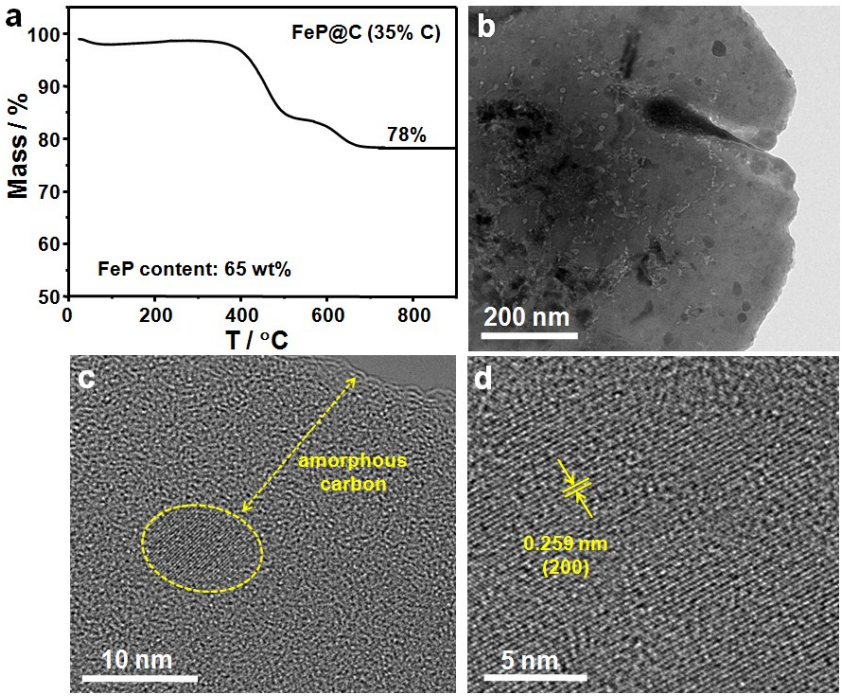

Figure S8. (a) TG curve, (b) TEM and (c,d) HR-TEM images of FeP@C with 35 wt% carbon content

.

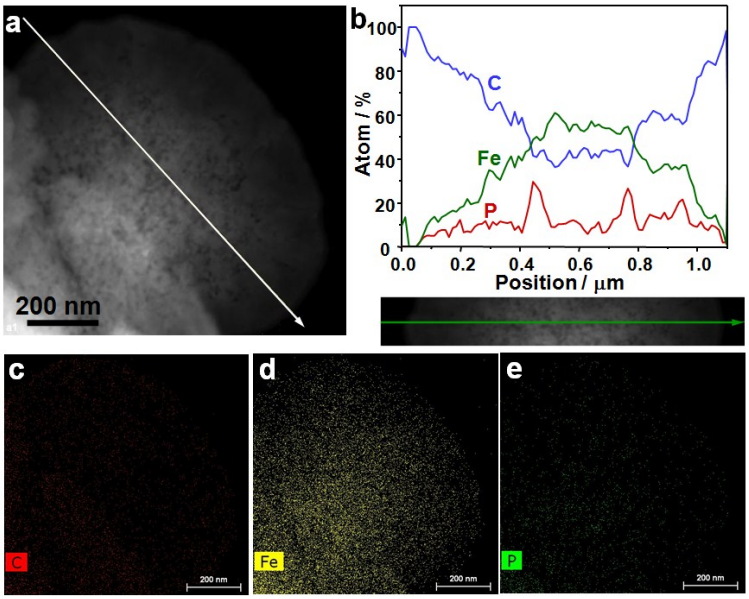

Figure S9. (a) STEM image and the corresponding carbon, iron, and phosphorus (b) EDS line-scan and (c-e) elemental mapping images of one FeP@C nanoplate.

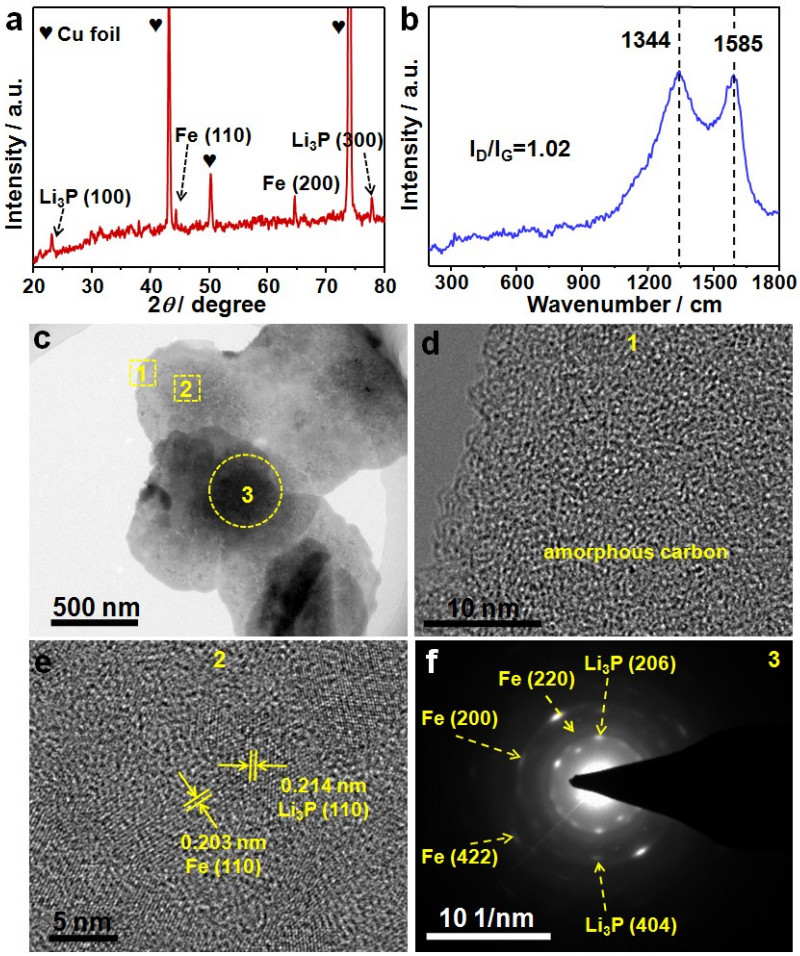

Figure S10. (a) XRD pattern, (b) Raman spectrum, (c) TEM, (d,f) HR-TEM images and (f) SAED pattern of FeP@C electrode after the first discharge.

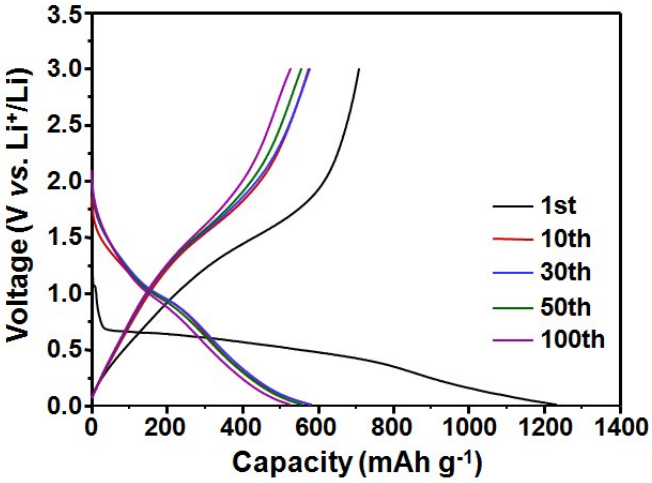

Figure S11. Galvanostatic discharge/charge profiles of Fe_3O_4@C nanoplates at a current density of 200 mA g^{-1}.

Table S1. Comparison of the electrochemical data of the FeP@C nanoplates and newly reported transition metal phosphide anodes for LIBs.

Electrode material	Current density (mA g^{-1})	Initial Coulombic Efficiency (%)	Reversible capacity (mAh g^{-1}) /Cycles	Capacity retention (%)	Reference
FeP@C nanoplates	200	70	720/100	96	This work
FeP@C nanorods	30	28	480/200	145	[1]
Fe_2P/carbon sheets	100	64	560/200	93	[2]
FeP_2/carbon nanotube	137	52	435/100	72	[3]
CuP_2/C	200	65	430/100	95	[4]
Hollow CoP/C	89	49	630/100	83	[5]
Peapod-like $Ni_{12}P_5$/C	100	50	620/100	92	[6]
Sandwiched NiP_2/graphene	108	62	625/200	92	[7]
C@Ni_3P/Ni/C	100	41	635/200	77	[8]
C@NiCoP peapods	200	77	670/350	95	[9]

Table S2. Fitted electrochemical impedance parameters of the FeP@C anodes.

Sample	R_e/Ohm	R_f/Ohm	R_{ct}/Ohm	Z_w/Ohm
fresh	6.88	10.53	61.45	53.41
after 1st cycle	5.14	7.43	18.62	71.48
after 50th cycle	7.25	18.46	31.48	89.19
after 100th cycle	7.42	19.59	28.76	82.13

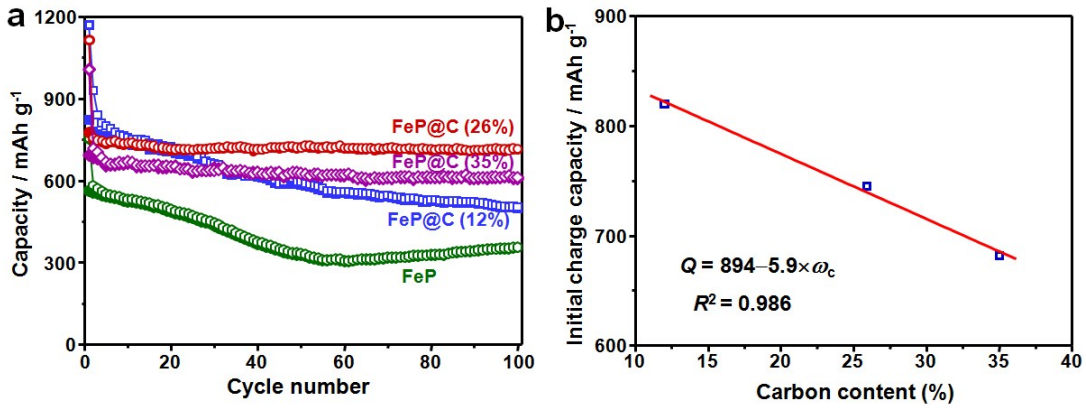

Figure S12. (a) Comparison of cycle performance of pure FeP and FeP@C with different carbon contents at a current density of 200 mA g^{-1}. (b) The relationship between initial charge capacity (Q) and the carbon content in FeP@C (ω_C).

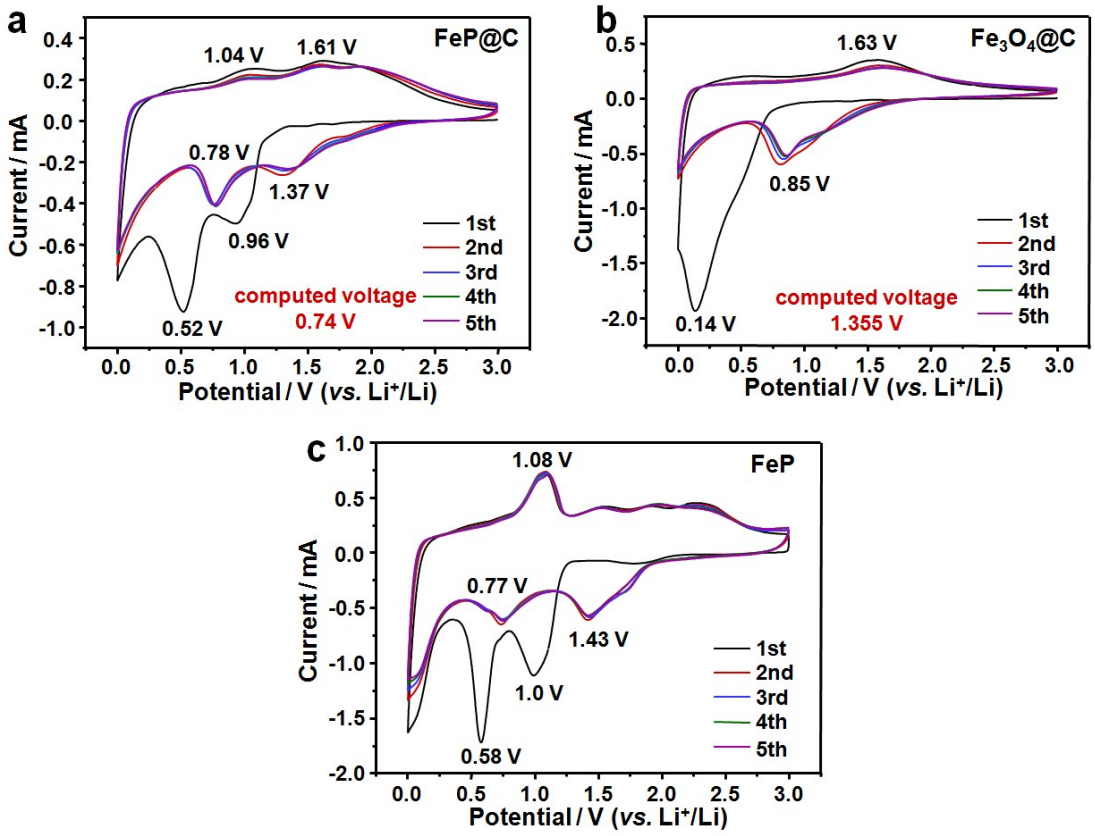

Figure S13. Cyclic voltammograms of (a) FeP@C, (b) Fe_3O_4@C and (c) pure FeP electrodes.

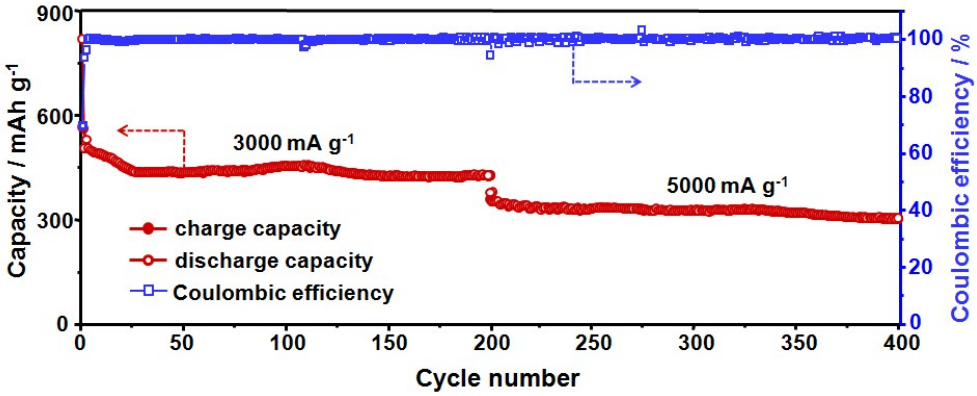

Figure S14. Long cycle performance of the FeP@C nanoplates at current densities of 3000 and 5000 mA g^{-1} for each 200 cycles.

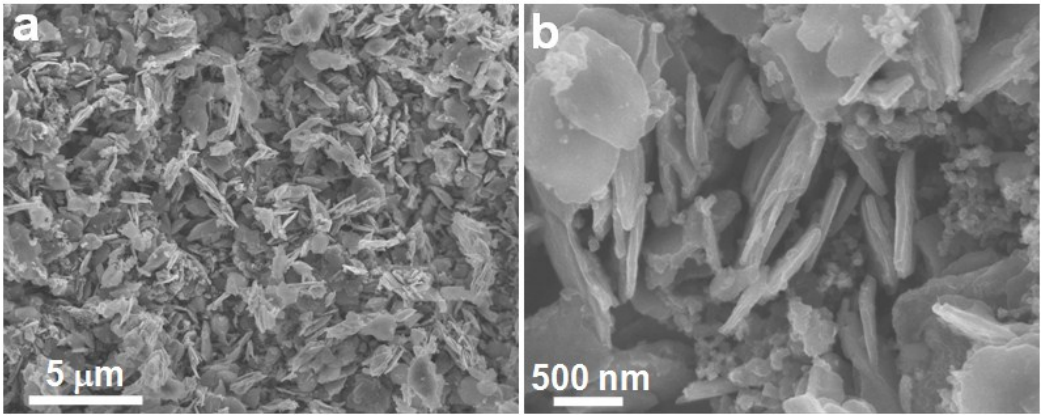

Figure S15. SEM images of FeP@C anodes after 50 fully charge/discharge cycles.

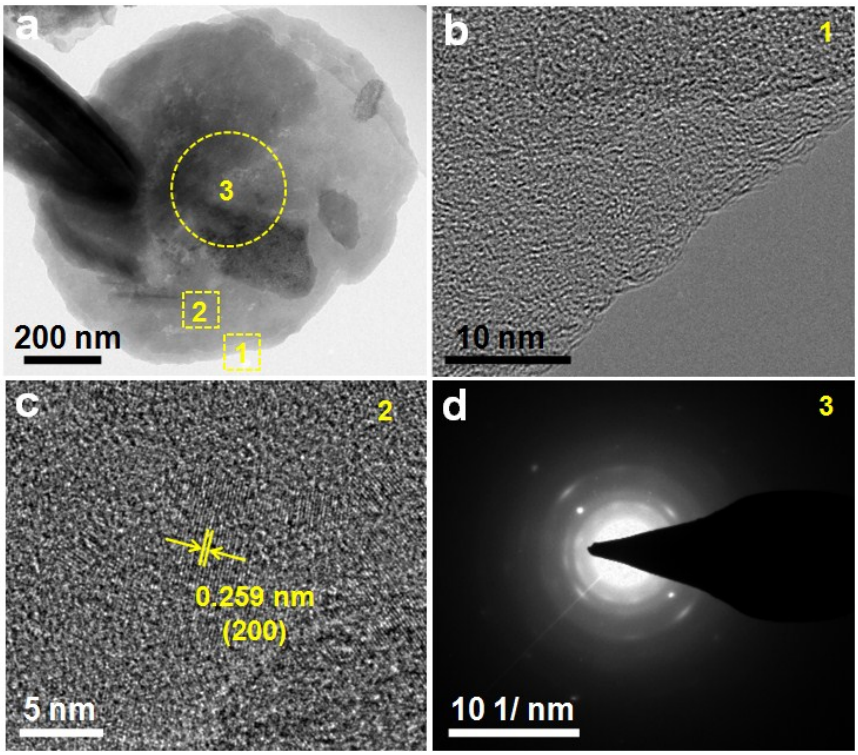

Figure S16. (a) TEM images of FeP@C anodes after 50 fully charge/discharge cycles. (b,c) Local-magnified TEM images of (1) and (2) areas, (d) SAED pattern of (3) area.

Reference

[1] J. Jiang, C. Wang, J. Liang, J. Zuo, Q. Yang, *Dalton Trans.*, 2015, **44**, 10297–10303.

[2] Y. Zhang, H. Zhang, Y. Feng, L. Liu, Y. Wang, *ACS Appl. Mater. Interfaces*, 2015, **7**, 26684–26690.

[3] J. Jiang, W. Wang, C. Wang, L. Zhang, K. Tang, J. Zuo, Q. Yang, *Electrochim. Acta*, 2015, **170**, 140–145.

[4] S.-O. Kim, A. Manthiram, *Chem. Commun.*, 2016, **52**, 4337–4340.

[5] D. Yang, J. Zhu, X. Rui, H. Tan, R. Cai, H. E. Hoster, D. Y. W. Yu, H. H. Hng, Q. Yan, *ACS Appl. Mater. Interfaces*, 2013, **5**, 1093–1099.

[6] H. Zhang, Y. Feng, Y. Zhang, L. Fang, W. Li, Q. Liu, K. Wu, Y. Wang, *ChemSusChem*, 2014, **7**, 2000–2006.

[7] Y. Feng, H. Zhang, Y. Mu, W. Li, J. Sun, K. Wu, Y. Wang, *Chem. Eur. J.*, 2015, **21**, 9229 –9235.

[8] Z. Liang, R. Huo, S. Yin, F. Zhang, S. Xu, *J. Mater. Chem. A*, 2014, **2**, 921–925.

[9] Y. Bai, H. Zhang, L. Liu, H. Xu, Y. Wang, *Chem. Eur. J.*, 2016, **22**, 1021–1029.